JOURNAL OF MATERIALS SCIENCE 22 (1987) 4111–4120

Impact properties of epoxy polymers

A. J. KINLOCH, G. A. KODOKIAN, M. B. JAMARANI
Department of Mechanical Engineering, Imperial College of Science and Technology, Exhibition Road, London, SW7 2BX, UK

Instrumented impact tests have been conducted on both a simple unmodified and a rubber-modified epoxy polymer over a range of impact velocities. Single-edge notched three-point bend and double-edge notched tensile specimens have been employed and, from the measured force–time response, values of the fracture energy, G_{Ic}, and the fracture toughness, K_{Ic}, have been determined and shown to be independent of the geometry of the test specimen. However, the measured value of the toughness is found to be dependent upon the impact velocity of the pendulum-striker and this dependence appears to largely arise from dynamic effects present in the test technique. The nature of these effects are discussed and modelled and the true 'material' impact resistance of the epoxy polymers determined. These studies clearly reveal that the multiphase microstructure of the rubber-modified epoxy leads to a significant improvement in the impact behaviour of cross-linked epoxy polymers.

1. Introduction

Epoxy polymers are typically highly cross-linked polymers and are widely used as the basis of structural adhesives and as matrices for fibre-composite materials. Previous studies [1–6] have concentrated upon the fracture behaviour of epoxy polymers under relatively slow strain-rates but, in both applications, a knowledge of the impact properties of the epoxy polymer is frequently of vital importance. The present paper is concerned with this aspect of the mechanical behaviour of such polymers.

The work described below was initiated with several aims. Firstly, to develop an instrumented impact test suitable for assessing the impact behaviour and, in particular, to establish whether a linear-elastic fracture-mechanics (LEFM) approach could be successfully adopted as a method for characterizing the impact resistance of epoxy polymers. Secondly, to investigate the effect of the impact velocity on the measured toughness of the epoxy polymers. Thirdly, to compare the impact behaviour of a multiphase rubber-toughened epoxy to that of a simple one-phase formulation. The former microstructure is known to increase the toughness of the material from tests conducted at relatively slow strain rates.

2. Theory

2.1. Linear-elastic fracture-mechanics (LEFM)

A basic aim of fracture mechanics is to identify fracture criteria such as the fracture energy, G_{Ic}, and fracture toughness, K_{Ic}, which are independent of the geometry of the cracked body. Values of such parameters should, therefore, greatly assist in developing a more fundamental understanding of the fracture process and be of considerable benefit in the practical areas of material formulation and selection and engineering design. Thus, to establish the validity of the LEFM approach two very different geometries of test specimen are examined in the present studies and the values of G_{Ic} and K_{Ic} are also ascertained over a very wide range of crack lengths. The geometries examined are the single-edge notched three-point bend and double-edge notched tensile specimens.

2.1.1. Single-edge notched three-point bend (SENB) specimen

The single-edge notched three-point bend (SENB) specimen is shown in Fig. 1. For a span/width ratio of 4, as employed in the present studies, the value of the fracture toughness or stress-intensity factor, K_{Ic}, at the onset of crack growth may be deduced [7] from the measured force, F_c, at crack initiation from the relation

$$K_{Ic} = (6F_c Ya^{1/2})/(BW) \quad (1)$$

where a is the length of a sharp crack, B is the thickness, W is the width of the specimen and Y is a dimensionless geometry factor which is given by

$$Y = \frac{(1.99 - \{a/W(1 - a/W)[2.15 - 3.93a/W + 2.7(a/W)^2]\})}{(1 + 2a/W)(1 - a/W)^{3/2}} \quad (2)$$

and these equations yield a value of K_{Ic} which is accurate to within $\pm 0.5\%$ over the entire range of a/W values.

The fracture energy, G_{Ic}, is given from a LEFM analysis by [8]

$$G_{Ic} = \frac{F_c^2}{2B}\frac{\partial C}{\partial a} \quad (3)$$

where C is the compliance of the test specimen and is defined by the displacement/load (i.e. u/F). If a dimensionless geometry factor, ϕ, is introduced such that [9]

$$\phi = \frac{C}{\partial C/\partial(a/W)} \quad (4)$$

0022–2461/87 $03.00 + .12

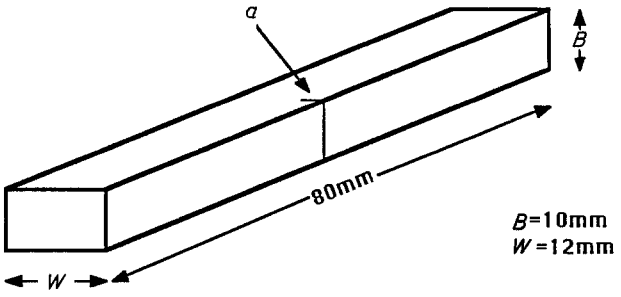

Figure 1 Sketch of single-edge notched three-point bend (SENB) specimen.

then it may be readily shown that [10]

$$G_{Ic} = \frac{U_c}{BW\phi} \tag{5}$$

where U_c is the stored elastic strain energy in the specimen at the onset of crack growth. The value of ϕ may be evaluated either from measuring the compliance as a function of crack length or, more readily, from published tables [10] of the value of ϕ as a function of a/W and L/W, where L is the length or span of the test specimen between the support points.

The values of K_{Ic} and G_{Ic} may also, of course, be related via the modulus of the material namely, [8]

$$K_{Ic}^2 = \frac{EG_{Ic}}{(1 - \nu^2)} \tag{6}$$

for plane strain, where ν is Poisson's ratio. The modulus may be determined from the compliance, C, where [11]

$$E = \frac{1}{BC}\{19.12 + 24[a/W/(1 - a/W)]^2 \times [5.58 - 19.57(a/W) + 36.82(a/W)^2 - 34.95(a/W)^3 + 12.77(a/W)^4]\} \tag{7}$$

However, a particular problem with polymeric materials is that the value of the modulus, E, is often dependent upon the test rate and it is therefore useful to be able to directly deduce values of both K_{Ic} and G_{Ic} without needing to determine the exact value of E.

2.1.2. The double-edge notched tensile (DEN) specimen

The double-edge notched tensile (DEN) specimen is shown in Fig. 2 and the value of K_{Ic} is given by [8, 12]

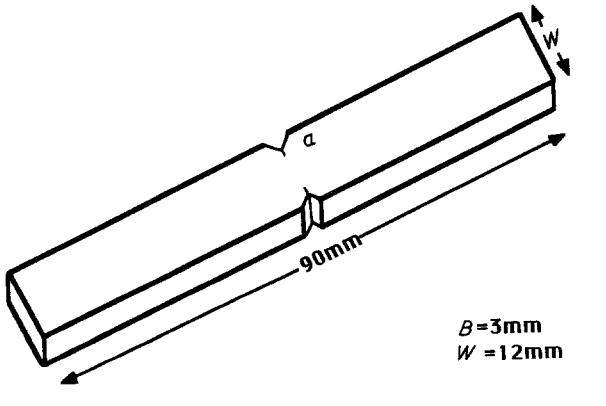

Figure 2 Sketch of double-edge notched (DEN) tensile specimen.

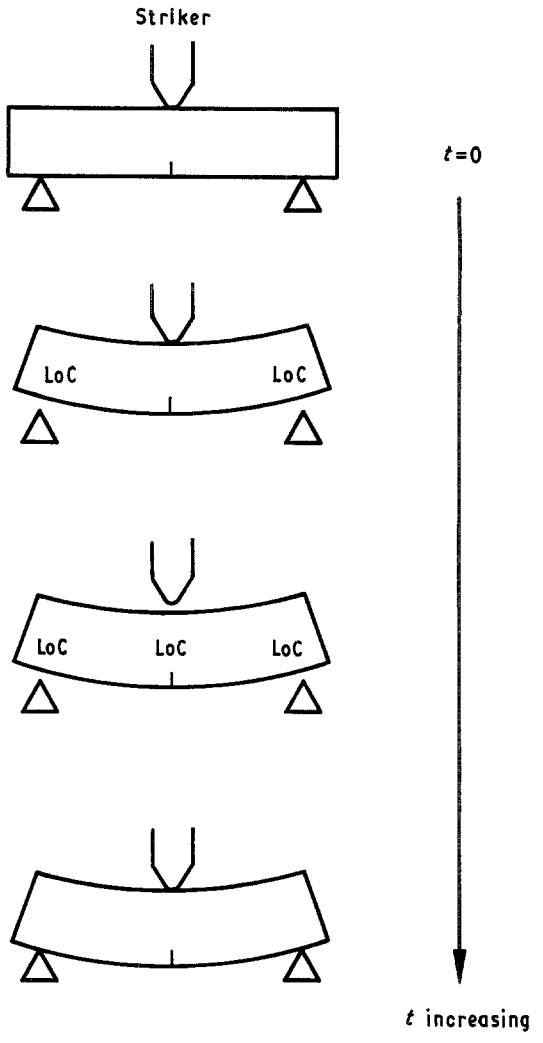

Figure 3 Sketch of dynamic effects leading to loss of contact (LoC) of SENB specimen with both striker and shoulders of vice.

$$K_{Ic} = (F_c Y a^{1/2})/(BW) \tag{8}$$

where the value of Y is given by

$$Y = 1.98 + 0.354(a/W) - 2.121(a/W)^2 + 3.422(a/W)^3 \tag{9}$$

and this expression for Y is accurate to within $\pm 4\%$ for $0 \leqslant a/W \leqslant 0.35$ and $L/W \geqslant 3$.

2.2. Dynamic effects

A most common form of impact testing is for a pendulum striker or hammer to be allowed to impact upon a supported bar, as indicated in Fig. 3. Further, many types of instrumented impact devices, such as that employed in the present studies, have the force-measuring transducer mounted on the pendulum-striker. It is therefore most important to recognize that the forces actually measured are those acting on the striker, and the energy deduced from such measurements is that lost by the striker. However, for the calculation of the true "material property" values of the impact fracture toughness and fracture energy from the above equations, the force that is needed is that acting in the specimen and the energy needed is that gained by the specimen. The problem that arises is that the measured values are not necessarily the

same as the values required. At relatively slow impact velocities differences between the measured values and those actually acting in the specimen may be negligible but differences may become very pronounced as the impact velocity of the striker is increased.

The above aspects have been convincingly demonstrated by the work of Kalthoff [13] and Williams and Adams [14] and arise from various dynamic effects associated with the test method. One such effect is the reflection of elastic stress waves which may interact with the propagating crack, but in impact tests such as those described in the present paper the time-scale of the impact event is long relative to the time taken for reflection of elastic stress waves and such effects do not have a dominating influence on the measured results. Other dynamic effects, which are important, arise from (i) the relatively high contact stiffness of the striker/specimen interface compared to that of the specimen, and (ii) the loss of contact and the regaining of contact between the specimen and the striker and the specimen and the shoulders of the mounting vice during the impact test. Such losses of contact have been observed directly by Kalthoff [13] and are shown schematically in Fig. 3. The loss of contact occurs due to the specimen accelerating and decelerating relative to the striker and also, associated with these changes in the displacement of the specimen, changes occur in the kinetic energy of the specimen. The important consequence of these dynamic effects is that because the force transducer is mounted on the striker, the bending forces and associated stored strain energy actually acting in the specimen may be incorrectly deduced. Also, severe oscillations and even multiple zero values may be observed in the measured force–time relationship.

Hence, the measured force–time relationship is complex and two basic problems arise. Firstly, it may be difficult to ascertain the particular point on the relationship which corresponds to the onset of crack initiation; in the present work a crack initiation gauge is used to overcome this problem. Secondly, the measured force at the onset of crack growth and the measured energy, ascertained by integrating the measured force–displacement relation, are not necessarily equivalent to the force or stored strain energy acting in the specimen. In the present studies this problem is at first avoided, by using only relatively low impact velocities which result in relatively long time-scales for the impact event and so enable such effects to be neglected at the instant of crack initiation. However, when higher impact velocities are examined, and the associated time-scale of the impact test is relatively short, dynamic effects may then be significant and are modelled using the theories recently advanced by Williams and Adams [14].

In order to model quantitatively the dynamic effects

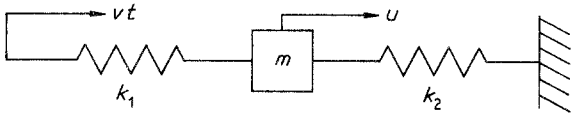

Figure 4 The dynamic model [14].

mentioned above, Williams and Adams [14] have proposed an analysis which treats the SENB specimen as a spring of stiffness $k_2(a)$ and an equivalent mass m, as shown schematically in Fig. 4. An important aspect of the model is that the contact stiffness, k_1, is introduced and this factor controls the dynamics of the system. The equation of motion for m is given

$$\text{mass} \times \text{acceleration} = \text{force in the direction of acceleration} \quad (10)$$

and therefore, from Fig. 4

$$m\ddot{u} = -k_2u - k_1(u - vt) \quad (11)$$

where the displacement of the mass is u and the striker moves with a constant velocity, v. Upon rearranging

$$m\ddot{u} + (k_1 + k_2)u = k_1vt \quad (12)$$

with the initial conditions $u = \dot{u} = 0$ at $t = 0$, then

$$u = \frac{k_1}{(k_1 + k_2)}\left[v\left(t - \frac{\sin \omega t}{\omega}\right)\right] \quad (13)$$

where ω is the natural frequency of the system, and

$$\omega^2 = \frac{(k_1 + k_2)}{m} \quad (14)$$

Using this model Williams and Adams [14] have demonstrated that if the force–time relation is ascertained by mounting the force transducer on the striker then oscillations in the measured force would be expected and that such oscillations will be particularly pronounced when the impact event lasts only for a very short time-scale, i.e. at high impact velocities. Indeed, the measured force may be an order of magnitude higher than the true force acting in the specimen. On the other hand, the measured force on the striker may be zero when forces are still present in the specimen, because of complete loss of contact of the striker with the specimen. Therefore, if the measured force–time relation is used to ascertain either the value of K_{Ic} or G_{Ic} then these values would be expected to be dependent upon the initial striker velocity, when the velocity is relatively high and the associated time-scale, t_f, is relatively short.

Obviously, it is most important to recognize and allow for such dynamic effects arising from the test method if the true material behaviour under impact velocities is to be isolated and understood. The model predicts that the true impact fracture energy, G_{Ic}^d, corrected for dynamic effects will be given by

$$G_{Ic}^d = \frac{U_c}{BW\phi}\left(\frac{\alpha}{\alpha + 1}\right)\frac{f(\chi)}{\{1 - 2\alpha/\chi^2(\cos \chi - 1)\}} \quad (15)$$

The first term on the right-hand side of Equation 15 is equivalent to the measured value of the fracture energy, G_{Ic}. This is determined by ascertaining the energy lost by the striker from the experimentally measured force–time relation and by then equating the energy lost by the striker to the energy stored in the specimen at the onset of crack growth; i.e. taking the energy deduced from the measured force–time relation up to the point of crack initiation as being equal to the value of U_c in Equation 5, as is the usual

procedure in interpreting impact test results. The second term in Equation 5 arises from variations in the deformation of the specimen and the third term is a consequence of changes in the kinetic energy in the specimen. The various parameters are defined by

$$\alpha = k_1/k_2 \quad (16)$$

$$\chi = \omega t_f \quad (17)$$

where t_f is the time-to-failure, i.e. the time taken from $F = 0$ to $F = F_c$, and

$$f(\chi) = \left(1 - \frac{\sin \chi}{\chi}\right)^2 + 4\left(\frac{1 - \cos \chi}{\chi}\right) \times \left[0.5 \sin \chi - \left(\frac{1 - \cos \chi}{\chi}\right)\right] \quad (18)$$

The value of the fracture energy, G_{Ic}, which will be determined from the measured force–displacement relation via Equation 5 and includes any dynamic effects, may be predicted from re-arranging Equation 15 to give

$$G_{Ic} = G_{Ic}^{d}\left(\frac{\alpha + 1}{\alpha}\right)\frac{[1 - 2\alpha/\chi^2(\cos \chi - 1)]}{f(\chi)} \quad (19)$$

3. Experimental details

3.1. Materials

The epoxy polymers examined in the present study have been model materials based upon a simple unmodified and a rubber-toughened epoxy resin. The epoxy resin employed was derived from the reaction of bisphenol A and epichlorohydrin and was largely composed of the diglycidyl ether of bisphenol A (DGEBA). The curing agent was piperidine. The rubber used to prepare the multiphase, rubber-modified epoxy adhesive was a carboxyl-terminated, random copolymer of butadiene and acrylonitrile (CTBN rubber: carboxyl content 2.37 wt/wt %; molecular weight 3500 g mol^{-1}). The formulations of the epoxy polymer are shown in Table I.

To prepare sheets of the rubber-modified epoxy the CTBN rubber was added to the epoxy resin and hand-mixed for approximately 5 to 10 min. This mixture was then heated to 65 ± 5° C in a water bath and mixed for 5 min using an electric stirrer and then degassed in a vacuum oven at 60° C until frothing stopped. When the mixture had cooled to below 30° C the piperidine was mixed in gently to minimise air entrapment. The rubber–epoxy mixture was then poured into a preheated mould, cured at 120° C for 16 h and allowed to cool slowly. The unmodified epoxy was prepared in the same manner without the addition of rubber. The formulation and cure schedule described above results [2, 5] in the rubber-modified material having a two-phase microstructure with a volume fraction of rubbery particles of 0.18 with an average particle size of 1.6 μm. The glass transition temperature of the epoxy is 100 ± 2° C.

TABLE I Formulations of epoxy adhesives

	Unmodified epoxy (p.h.r.*)	Rubber-modified epoxy (p.h.r.)
DGEBA epoxy resin	100	100
Piperidine	5	5
CTBN rubber	–	15

*p.h.r. = parts per hundred of resin.

3.2. Preparation of test specimens

The SENB specimens were prepared by casting sheets of the epoxy polymers as described above which were 10 mm thick and then machining bars to the dimensions shown in Fig. 1. The DEN specimens were machined to the dimensions shown in Fig. 2 from sheets which had been cast to give a thickness of 3 mm. In both cases sharp cracks were inserted in the positions shown in Figs 2 and 3, respectively, by first machining a notch of radius approximately 12 μm and then gently tapping a fresh razor blade into the notch so as to propagate a sharp, natural crack ahead of the razor blade. Cracks of various lengths, a, were inserted using this technique.

Most of the test specimens had a crack initiation gauge applied to one surface so that the onset of crack growth, and the associated force at this point, could be accurately determined. The design of the gauge followed closely that described by Beguelin *et al.* [15]. One face of the specimen, of width W and perpendicular to the face across which the crack was inserted, was drilled to accommodate two small electrical pins, which were pushed into place one on each side of the crack and about 10 mm from the crack. Then a graphite polymeric-based film was sprayed completely across the width of the specimen to give a thin, uniform graphite film to a distance of about 1.5 to 2 mm on either side of the crack. The gauge was finished by painting a thin line of conductive silver paint over the top of the far edge of the graphite layer, i.e. completely across the width of the specimen, and then on each side of the crack a silver-paint connecting path was painted to the electrical pin which had been mounted on that half of the specimen.

3.3. The instrumented impact test

3.3.1. The equipment

The impact tests were conducted using a commercial instrumented machine (Ceast, Turin, Italy). It essentially consisted of a pendulum-striker which was allowed to impact against the specimen. The velocity with which the striker impacted against the specimen could be varied by changing the angle from which the striker was released. The initial studies were conducted using relatively low impact velocities of about 0.3 to 1 msec^{-1} which resulted in times-to-failure, t_f, of about 750 μsec to 1 msec. Subsequent studies were conducted using higher impact velocities up to about 3.5 msec^{-1} when values of t_f down to about 100 μsec were recorded. Depending upon the type of specimen which was employed, the strain-gauge transducer was either mounted in the striker or in the vice in which the specimen was gripped, as discussed below. In either case the force transducer was connected to a transient recorder and therefore, via a prior static calibration, the impact force–time signal could be obtained. The memory module received the signal, converted by the

analogue/digital converter into digital form, and stored these data. The time-base generator was based upon intervals of 2-4-8-16-32-64-124-256 msec and each of these was divided into 2016 points so that the time interval between two bits (information) was included between 1 and 126 μsec. By adjusting the trigger system according to the duration of the phenomenon, the memory module could store the complete force–time history of the impact experiment. These data could be accessed by the dedicated microcomputer. It should be noted that throughout these studies no filtering of the force–time signal was performed, because although the equipment had this capability, it was considered that vital information might be lost by such an operation.

As mentioned above, it was also considered to be essential to be able to discern the point on the measured force–time curve that the inserted crack began to propagate. To determine this point the crack initiation gauge was connected to a balancing bridge which gave a constant voltage. The signals from both the balancing bridge and the transient recorder which was used to store the force–time data were connected to a second transient recorder to produce, on the same time-scale axis, both changes in the force (from the semi-conductor strain gauge) and resistance (from the crack initiation gauge) as a function of time. These data could be accessed via an X–Y plotter.

3.3.2. The SENB tests

The SENB specimen was placed on the shoulders of the vice of the instrumented impact machine to give a span of 48 mm and was struck by the pendulum-striker on the reverse face to that containing the inserted crack. The strain-gauge transducer was mounted in the tup of the pendulum-striker and a record of the force on the tup against time and resistance of the crack initiation gauge against time were recorded as described above. Apart from enabling direct graphical representation of the striker force–time data, the computer was programmed to deduce various other parameters of interest. The equations used were simply based upon Newtonian mechanics and required a knowledge of the initial impact velocity and the mass of the pendulum-striker. The equations used in the program yielded (i) the energy lost by the striker as a function of time, (ii) the displacement of the striker as a function of time, and (iii) the striker force–displacement relation. Assuming that no dynamic effects, such as those described earlier, are experienced then the values of these various parameters may also be taken to be those relevant to the specimen. This is the usual assumption and the values of K_{Ic} and G_{Ic} referred to in the present paper as "measured" values are calculated from Equations 1 to 9 on this basis. However, as shown later, only at the lowest impact velocities were the impact tests essentially free from dynamic effects.

3.3.3. The DEN tests

In the case of the DEN specimens, the end of a specimen was gripped in the vice mounted on the impact machine and the vice contained the strain-gauge transducer. A bar, wider than the specimen, was firmly bolted on to the other end of the specimen to give a length of DEN specimen of 60 mm between the loading points. A non-instrumented U-shaped pendulum-striker was employed and as this striker passed the lowest point of its swing it impacted against the bar bolted to the far end of the DEN specimen and so caused the specimen to be subjected to an applied uniaxial tensile force. The force–time curve and resistance of the crack initiation gauge–time data were stored and recorded as described above. The values of the measured force at the onset of crack growth were used to calculate the value of K_{Ic} from Equations 8 and 9.

4. Results and discussion

4.1. SENB tests – low impact velocities

Typical measured force–time (from the transducer on the striker) and corresponding resistance–time (from the crack initiation gauge) relations are shown in Fig. 5 for the SENB specimens tested at a low impact velocity, i.e. 0.5 msec^{-1}. It may be seen that the force–time relation is relatively free from oscillations arising from dynamic effects and that the crack initiation gauge reveals that there is no substantial change in resistance, and hence no crack growth, until the maximum load is attained. From such data it is therefore possible to ascertain the point of crack initiation and, also, the value of the time-to-failure, t_f, where t_f is defined as the time taken for the value of the measured force to increase from $F = 0$, at the start of the force–time curve, to $F = F_c$ when the onset of crack growth occurs.

The above experiment was repeated for specimens containing various lengths of cracks. To determine the value of the fracture toughness, K_{Ic}, and to

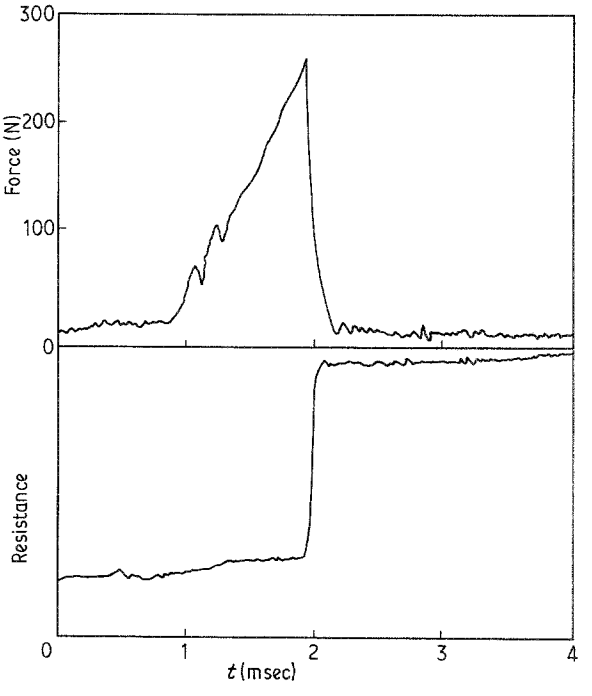

Figure 5 Force against time (from the striker transducer) and resistance versus time (from the crack initiation gauge) traces for the SENB rubber-modified epoxy polymer. (Striker velocity 0.5 m sec^{-1}.)

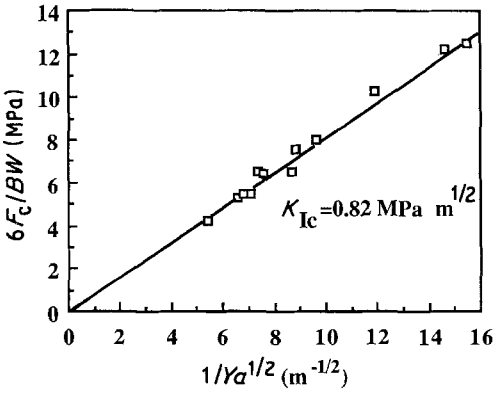

Figure 6 Results plotted in the form of Equation 1 for the unmodified epoxy SENB specimens with a striker velocity of 0.33 m sec^{-1}, giving a t_f of 800 μsec.

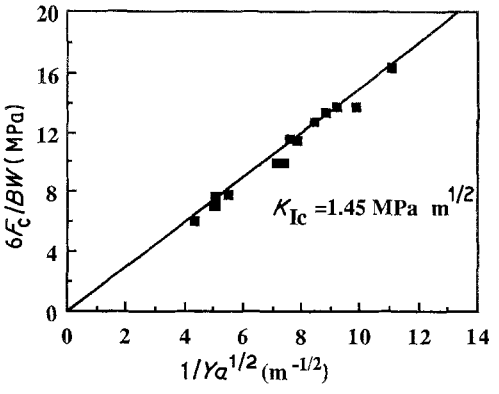

Figure 7 Results plotted in the form of Equation 1 for the rubber-modified epoxy SENB specimens with a striker velocity of 0.5 m sec^{-1}, giving a t_f of 930 μsec.

ascertain its independence upon the value of the crack length employed, the term $6F_c/BW$ is plotted against $1/Ya^{1/2}$ in Figs 6 and 7 for the unmodified and rubber-modified epoxy polymers, respectively. In both cases a good linear relation is expected which yields, from Equation 1, values of K_{Ic} which are independent of crack length. The values of K_{Ic} are shown in Table II.

The measured force–time relations were also used to obtain the energy, U_c, at the onset of crack growth and again values of this parameter were obtained as a function of the crack length for both the unmodified and rubber-modified materials. Values of U_c are plotted against the respective values of $BW\phi$ in Figs 8 and 9 for these epoxy polymers. From Equation 5 a linear relationship passing through the origin would be expected if the value of G_{Ic} is independent of crack length, as is indeed observed. The values of G_{Ic} are given in Table II.

Finally, the value of G_{Ic} may also be calculated from the value of K_{Ic} and a knowledge of the modulus, E, using Equation 6. The modulus of the epoxy materials under impact loading was ascertained by determining the force–displacement relation for the SENB specimens, and so deducing the compliance, C, of the specimen, and then using Equation 7 to calculate the value of E. The values of modulus so deduced are 1.68 and 1.65 GPa for the unmodified and rubber-modified materials, respectively. The value of ν in Equation 6 was taken to be 0.35. The values of G_{Ic} so determined are shown in Table II and are in good agreement with those derived from Equation 5.

4.2. DEN – low impact velocities

The force, F_c, at the onset of crack growth was determined as described previously and values of F_c/BW are plotted against $1/Ya^{1/2}$ in Figs 10 and 11 for the unmodified and rubber-modified epoxy polymers, respectively. As may be seen, a linear relation is obtained, as expected from Equation 8, and the value of K_{Ic}, and the corresponding value of G_{Ic} from Equation 6, are in good agreement with the values determined using the SENB specimen.

Thus, the values of K_{Ic} and G_{Ic} for the epoxy polymers are independent of the details of the test geometry and the method of analysis and these observations confirm the applicability of a LEFM approach.

4.3. Dynamic effects

The SENB specimen was employed to investigate the effect of increasing the striker velocity on the impact behaviour. As the impact velocity is increased the measured force–time relation shows an increasing number of oscillations with even zero values of the force being recorded. The pronounced form of the oscillations that may be recorded may be seen from the experimental relation shown in Fig. 12. As discussed earlier, such oscillations arise from the relatively high contact stiffness of the striker/specimen interface and the acceleration and deceleration of the specimen relative to the striker. Hence, the force measured by the transducer mounted on the striker fluctuates accordingly. Indeed, at the highest velocities the specimen may even lose contact with the striker and hence the measured force becomes zero.

The dynamic effects which occur at the higher impact velocities are clearly evident on the force–time relation, as may be seen from Fig. 12. However, in

TABLE II Values of the fracture toughness, K_{Ic}, and the fracture energy, G_{Ic}, at low impact velocities

Impact velocity (m sec^{-1})	Specimen	t_f (μsec)	K_{Ic} (MPa m$^{1/2}$)	G_{Ic}(Eq. 5) (kJ m^{-2})	G_{Ic}(Eq. 6) (kJ m^{-2})
Unmodified epoxy					
0.33	SENB	800	0.82	0.48	0.35
0.83	DEN	625	1.10	–	0.62
Rubber-modified epoxy					
0.50	SENB	930	1.45	1.38	1.12
0.99	DEN	750	1.61	–	1.38

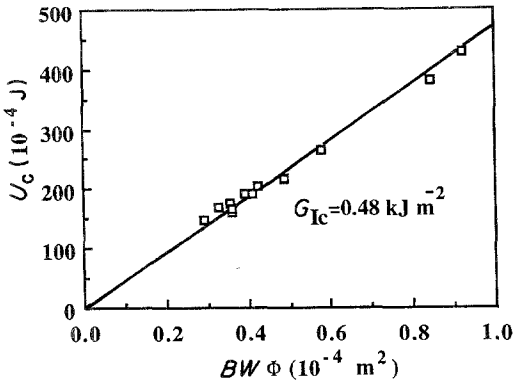

Figure 8 Results plotted in the form of Equation 5 for the unmodified epoxy SENB specimens with a striker velocity of 0.33 m sec^{-1}, giving a t_f of 800 μsec.

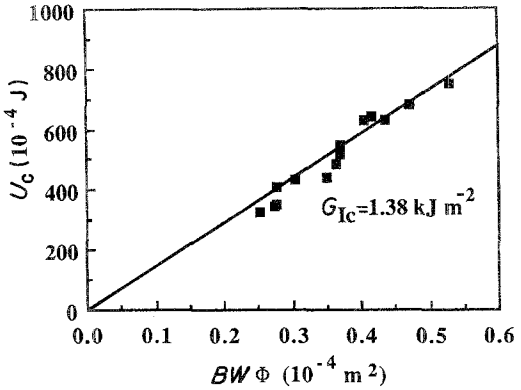

Figure 9 Results plotted in the form of Equation 5 for the rubber-modified epoxy SENB specimens with a striker velocity of 0.5 m sec^{-1}, giving a t_f of 930 μsec.

most instances the crack initiation gauge does enable the point of crack growth to be clearly identified. For example, in Fig. 12 the onset of crack initiation is not at the first peak, which arises from dynamic effects associated with the test method, but occurs at the second peak in this particular case. Therefore, the measured energy, U_c, may be deduced and the value of the fracture energy, G_{Ic}, determined from Equation 5. Also, the value of the time-to-failure, t_f, may be readily ascertained. Values of G_{Ic} against t_f so determined are shown in Figs 13 and 14 for the unmodified and rubber-modified materials, respectively. Obviously, the data at lower values of t_f are obtained essentially from employing the higher striker velocities. The dramatic effect that reducing the time-scale of the impact event has upon the measured fracture energy is clearly visible and, from simply using the measured energy, U_c, to deduce the value of G_{Ic}, it appears that the material is actually *tougher* at the shorter time-scales, i.e. under the highest impact velocities. Intuitively this would not be expected from a materials science standpoint.

Now Equation 19 may be used to predict theoretically the form of the G_{Ic}–t_f relation. It will be recalled that the model which this equation describes assumes that a variation of the measured G_{Ic} value with t_f will result from the dynamic effects which are evident in the measured force–time relation, as discussed above. In this equation the values of the effective mass, m, the contact stiffness, k_1, and specimen stiffness, k_2, may be readily determined and therefore the parameters ω, α and χ may be calculated. The effective mass is simply [16] the mass of the specimen multiplied by 17/35. The contact stiffness, k_1, was measured by supporting the SENB specimen on a steel block and allowing the instrumented striker to bounce against the specimen and from the measured force–displacement curve the value of k_1 was deduced. The stiffness of the specimen, k_2, is a function of the crack length and therefore two values were taken to give bounds to the theoretical predictions of G_{Ic}–t_f. One bound was deduced by taking the value of the specimen stiffness at the maximum value of a employed in the tests, i.e. $a = a$ (max); the value of a (max) was 4.8 mm in the case of the unmodified and 3.0 mm for the rubber-modified epoxy specimens. The other bound was calculated assuming $a \rightarrow 0$. The values of k_2 were determined experimentally from the slope of the force–displacement relation. The values of the various parameters used in the model are shown in Tables IIIa and IIIb.

It is also of interest to calculate values of the specimen stiffness, k_2, and compare such values to those measured experimentally, which are shown in Tables IIIa and IIIb. The value of the specimen stiffness, k_2, at $a = 0$ may be deduced from a knowledge of the material's modulus, E, using the relation

$$k_2(a = 0) = 4EBW^3/L^3 \tag{20}$$

whilst at $k_2[a = a(\text{max})]$ the value is given by (see Appendix)

$$k_2[a = a(\text{max})] = \left[\frac{1}{18}\frac{L/W}{\phi Y^2(a/W)}\right] k_2(a = 0) \tag{21}$$

where Y is given by Equation 2. For the unmodified and rubber-modified epoxy specimens the theoretical values for $k_2(a = 0)$ are 1.05 and 1.03 MN m^{-1},

TABLE III (a) Values of the various parameters employed in the dynamic modelling for $a \rightarrow 0$

Material	m (g)	k_1 (MN m^{-1})	k_2 (MN m^{-1})	ω (krad sec^{-1})	α	G_{Ic}^d (kJ m^{-2})
Unmodified epoxy	5.5	6.50	1.15	37.3	5.65	0.41
Rubber-modified epoxy	5.7	5.45	0.97	33.6	5.62	1.38

(b) Values of the various parameters employed in the dynamic modelling for $a = a$(max)

Material	m (g)	k_1 (MN m^{-1})	k_2 (MN m^{-1})	ω (krad sec^{-1})	α	G_{Ic}^d (kJ m^{-2})
Unmodified epoxy	5.5	6.50	0.56	35.8	11.61	0.41
Rubber-modified epoxy	5.7	5.45	0.67	32.7	8.13	1.38

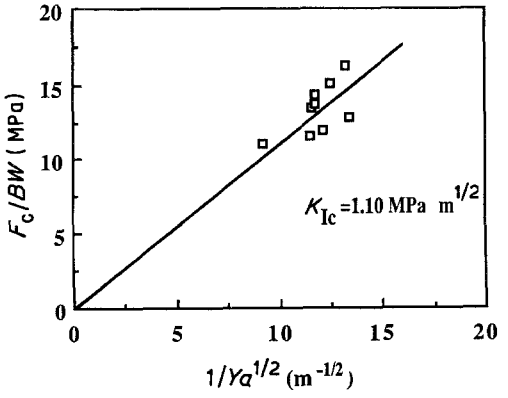

Figure 10 Results plotted in the form of Equation 8 for the unmodified epoxy DEN specimens with a striker velocity of 0.83 m sec^{-1}, giving a t_f of 625 μsec.

respectively, and for $k_2[a = a\,(\max)]$ are 0.51 and 0.67 MN m^{-1}, respectively. These values are in very good agreement with the experimental values shown in Tables IIIa and b, thus confirming the experimental studies.

Finally, to use Equation 19, values of the true "material" impact fracture energy, G_{Ic}^{d}, are required. Values of G_{Ic}^{d} of 0.41 and 1.38 kJ m^{-2} have been deduced by fitting the experimental data to Equation 19. Independent support for these values comes from the observation that they are in very close agreement with the values of the fracture energy, G_{Ic}, which were experimentally determined for these materials under relatively slow-velocity impact tests (see Table II) – under such impact tests the dynamic effects which are presently being modelled have been found to be negligible.

The values of the various parameters listed in Table IIIa and b have been used in Equation 19 to predict the influence of dynamic effects on the measured value of G_{Ic} as a function of the time-to-failure, t_f. The theoretical predictions, together with the experimental points, are shown in Figs 13 and 14 and the agreement between the theoretical predictions and the experimental data is extremely good and this raises several interesting discussion points.

Firstly, the theoretical relationship is dependent upon the value of the specimen stiffness, k_2, and the upper and lower bounds are indicated in Figs 13 and

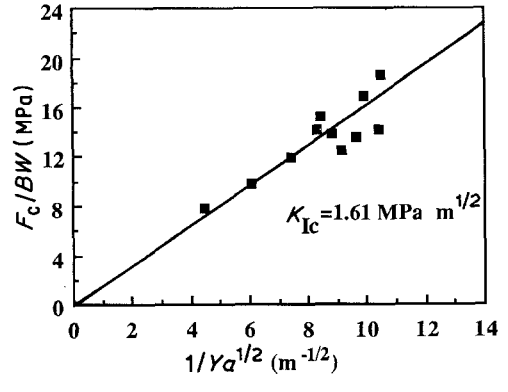

Figure 11 Results plotted in the form of Equation 8 for the rubber-modified epoxy DEN specimens with a striker velocity of 0.99 m sec^{-1}, giving a t_f of 750 μsec.

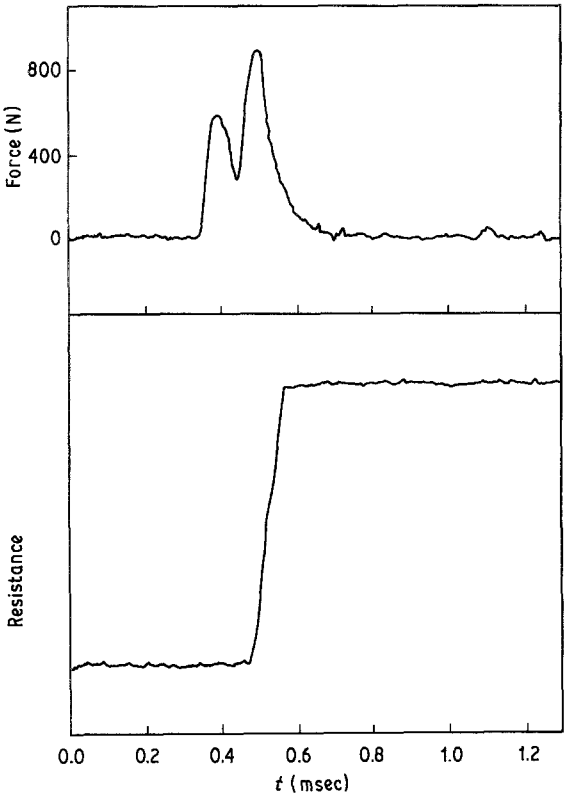

Figure 12 Force against time (from the striker transducer) and resistance against time (from the crack initiation gauge) traces for the SENB rubber-modified epoxy polymer. (Striker velocity 3.47 m sec^{-1}.)

14. Secondly, the theoretical relationships predict that at very low values of t_f, typically less than about 150 to 175 μsec, the measured value of G_{Ic} will rapidly rise. Thus, the observed increases in G_{Ic} at the higher impact velocities appear to arise from dynamic effects, and this effect is *not*, therefore, an inherent property of the materials. Indeed, the good fit of the theoretical relation, which models solely the dynamic effects, to the experimental data suggests that the true material property G_{Ic}^{d} values are not strongly dependent upon the value of t_f in the range currently explored, namely from about 100 μsec to 2 msec. Thirdly, the present data suggest that it is not necessary to invoke other mechanisms of impact fracture, such as thermal blunting [17], to account for the dependence of the

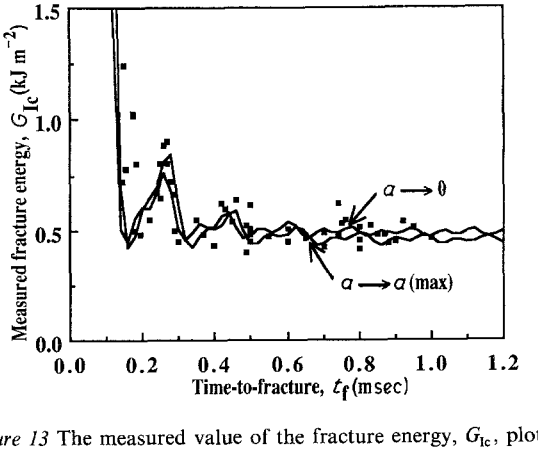

Figure 13 The measured value of the fracture energy, G_{Ic}, plotted against the time-to-failure, t_f, for the unmodified epoxy polymer. Points experimental, solid lines theoretical from Equation 19.

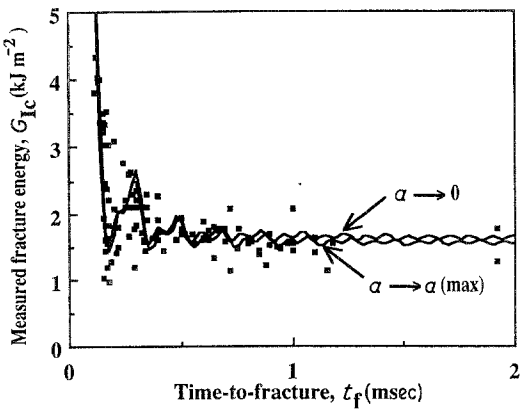

Figure 14 The measured value of the fracture energy, G_{Ic}, plotted against the time-to-failure, t_f, for the rubber-modified epoxy polymer. Points experimental, solid lines theoretical from Equation 19.

measured fracture energy upon the time-to-failure. Finally, the results shown in Figs 13 and 14 confirm that the true impact fracture energies, G_{Ic}^d, of the unmodified and rubber-modified epoxy polymers are about 0.4 and 1.4 kJ m^{-2}, respectively.

4.4. Effect of microstructure

From the above discussions it is evident that the true "material" impact toughness of the rubber-modified epoxy is significantly greater than that of the unmodified epoxy: the respective values of G_{Ic}^d being 1.4 and 0.4 kJ m^{-2}. This arises from the main energy-dissipating micromechanisms at the crack tip involving shear deformations in the epoxy [2, 6, 18]. The extent of such deformations are very limited in the unmodified material but occur over a large volume in the rubber-modified material, because many such deformations are initiated by the rubbery particles which are present in this multiphase polymer. The increased plastic and viscoelastic energy which is dissipated at the crack tip by this multiple-deformation micromechanism is reflected in an increase in the value of G_{Ic}^d. Indeed, the value of G_{Ic}^d for the rubber-modified polymer is about three to four times greater than the value for the unmodified material.

However, it should be noted that misleading results may be obtained if certain striker velocities are selected for the impact test. In a particular range of striker velocities an impact test on the intrinsically tougher rubber-modified epoxy may suffer none, or only very small, dynamic effects. On the other hand, under the same test conditions the unmodified epoxy, which is inherently far less tough, will have a lower time-to-failure. The lower value of t_f may lead to considerable dynamic effects being incurred during the impact test and hence a value of the fracture energy, G_{Ic}, being measured which is far higher than the true inherent value. Thus, to summarize, over a particular range of impact velocities dynamic effects may be present when testing the unmodified material but not the rubber-modified polymer, and this may lead to an incorrect assessment of both the absolute and relative true impact fracture energies of the materials.

5. Conclusions

The present studies have described the development of an instrumented impact test which has been used to study the crack growth in epoxy polymers under dynamic conditions. The impact test method has been used to examine the behaviour of an unmodified and rubber-toughened epoxy polymer and the results have clearly supported the use of a linear-elastic fracture-mechanics approach. Such an approach has been shown to yield values of the stress-intensity factor, K_{Ic}, at the onset of crack growth and the fracture energy, G_{Ic}.

However, except at the lowest striker velocities, which result in the longest times-to-failure, t_f, the measured value of G_{Ic} is highly dependent upon the impact velocity which is employed. This does not arise from any inherent material property of the polymers but is due to dynamic effects. These dynamic effects result from the relatively high contact stiffness of the striker/specimen interface and the acceleration and deceleration of the specimen relative to the striker, coupled with the force transducer being mounted in the tup of the striker. The force on the striker is therefore measured, rather than the force acting in the specimen. These dynamic effects have been successfully taken into account and the true "material" impact fracture energies of the epoxy polymers determined. The rubber-modified epoxy is shown to be inherently far tougher under impact conditions than the unmodified polymer.

Acknowledgements

The authors would like to acknowledge the financial support provided by the SERC through the Polymer Engineering Directorate and discussions on this work with Professor J. G. Williams.

Appendix

The stiffness, k_2, of the SENB specimen with a crack of length, a, may be deduced by first recalling that the value of G_{Ic} is given by Equation 3: $G_{Ic} = (F_c^2/2B)(\partial C/\partial a)$, but may also be expressed by [8, 10]

$$G_{Ic} = \frac{\sigma_c^2 Y^2 a}{E} \tag{A1}$$

where, for the SENB specimen the value of the stress, σ_c, at the onset of crack growth is given by:

$$\sigma_c = \frac{3F_c L}{2BW^2} \tag{A2}$$

Therefore from Equations 3, A1 and A2

$$\frac{\partial C}{\partial(a/W)} = \frac{9}{2}\frac{L^2 Y^2 a}{BW^3 E} \tag{A3}$$

But $k_2 = C^{-1}$, thus from Equation 4

$$k_2 = \frac{1}{\phi \partial C/\partial(a/W)} \tag{A4}$$

hence, from Equation A3

$$k_2 = \left(\frac{2}{9\phi Y^2 a/W}\right)\frac{EBW^2}{L^2} \tag{A5}$$

But for $a = 0$, Equation 20 gives $k_2(a = 0) = 4EBW^3/L^3$. Thus, substituting into Equation A5

from Equation 20 yields for $a = a(\max)$

$$k_2[a = a(\max)] = \left(\frac{1}{18}\frac{L/W}{\phi Y^2 a/W}\right) k_2(a = 0)$$

which is Equation 21.

References

1. W. D. BASCOM and R. L. COTTINGTON, *J. Adhesion* **7** (1976) 333.
2. A. J. KINLOCH, S. J. SHAW, D. A. TOD and D. L. HUNSTON, *Polymer* **24** (1983) 1341.
3. A. J. KINLOCH, S. J. SHAW and D. L. HUNSTON, *ibid.* **24** (1983) 1355.
4. A. J. KINLOCH, D. G. GILBERT and S. J. SHAW, *J. Mater. Sci.* **21** (1986) 1051.
5. A. J. KINLOCH and D. L. HUNSTON, *J. Mater. Sci. Lett.* **6** (1987) 137.
6. A. YEE and R. A. PEARSON, *J. Mater. Sci.* **21** (1986) 2462.
7. J. E. SRAWLEY, *Int. J. Fracture* **12** (1976) 475.
8. A. J. KINLOCH and R. J. YOUNG, "Fracture Behaviour of Polymers" (Applied Science, London, 1983) p. 79.
9. E. PLATI and J. G. WILLIAMS, *Polymer Engng Sci.* **15** (1975) 470.
10. J. G. WILLIAMS, "Fracture Mechanics of Polymers" (Ellis Horwood, Chichester, 1984) p. 68.
11. G. K. A. KODOKIAN, MSc thesis, Imperial College, University of London (1986) p. 15.
12. O. L. TOWERS and S. J. GARWOOD, *Weld. Res. Int.* **9** (1979) 56.
13. J. F. KALTHOFF, *Int. J. Fracture* **27** (1985) 277.
14. J. G. WILLIAMS and G. C. ADAMS, *ibid.* **33** (1987) 209.
15. P. H. BEGUELIN, B. STADLER and H. H. KAUSCH, *ibid.* **22** (1983) R47.
16. J. G. WILLIAMS, *ibid.* **33** (1987) 47.
17. J. G. WILLIAMS and J. M. HODGKINSON, *Proc. Roy. Soc. London* **A375** (1981) 231.
18. A. J. KINLOCH (ed.), "Structural Adhesives: Developments in Resins and Primers", (Elsevier Applied Science, London, 1986) p. 127.

Received 4 February
and accepted 15 April 1987